Adsorption-mediated nonlinearity of critical cracking thickness in drying nanoparticle polymer suspensions

doi: https://doi.org/10.1002/aic.17229

Adsorption-mediated Nonlinearity of Critical Cracking Thickness in Drying Nanoparticle–Polymer Suspensions

Masato Yamamura

Department of Applied Chemistry, Kyushu Institute of Technology, Kitakyushu, Japan, Corresponding author: yamamura@che.kyutech.ac.jp

Key words: drying, suspension, critical cracking thickness, polymer adsorption, stress

We examine the critical cracking thicknesses of as-dried colloidal TiO_2 suspensions containing water-soluble polymeric additives, above which cracks spontaneously propagate. In contrast to common observations, the critical cracking thickness increases in a non-linear, stepwise manner as increasing the concentration of polymeric additive in the suspension. The critical thickness diverges when the polymer content increases above a certain threshold. We demonstrate that the first and second critical cracking thickness increments are attributable to the onset of polymer adsorption and a subsequent transition in the conformations of the adsorbing polymer chains, respectively. The critical thickness profiles with respect to normalized polymer adsorption amounts at different particle diameters converged into a single master curve. These results illustrate nontrivial evaporation processes in which the various roles of polymeric additives delay cracking into thicker films.

Introduction

During the drying of thin films of a colloidal suspension coated on a solid substrate, capillary forces compress the particles when air–liquid interfaces retreat into a packed particle array [1]. The compressive stress relaxes as the coating bends or contact lines move to shrink the film along the solid surface. When the contact lines are pinned on a rigid substrate, the suspension resists the transverse deformation and promotes the development of in-plane tensile stresses, which often lead to radial [2], circular [3], zig-zag [4], star-shaped [5], or stripe [6-10] trajectories of cracks that can degrade the final quality of industrial coating applications, such as fuel-cell membrane electrode assemblies [11-12], flexible conductive films [13], paints, and cosmetics. Experimental studies on *in situ* stress measurements [14-21] and theoritical investigations on the contact and deformation of packing elastic particles [8, 22-25] are being conducted to address this issue.

According to the Griffith theory [26], the reduction in the elastic energy via crack opening overshadows the energy elevation by creating new interfaces when the crack length exceeds a critical value. Singh and Tirumkudulu [27] employed the Griffith's criterion to derive an expression for the critical stress (σ_c) of crack propagation, $\sigma_c \sim h^{-2/3}$, where h is the thickness at cracking, thereby suggesting that thinner films are less prone to cracking. It has been long known that cracks in colloidal suspensions spontaneously evolve only above a critical thickness, which is often referred to as the critical cracking thickness (h_{CCT}) [28-30] or maximum crack-free thickness.

However, there are conflicting reports as to whether polymeric additives delay or assist the onset of cracking. A pioneering work by Chiu et al. (1993) [28]

showed that the critical cracking thickness of an alumina suspension first decreased and then linearly increased with the concentration of polyvinyl alcohol (PVA) as an additive. In contrast, the critical thickness exhibited a maximum at a critical concentration of polyvinylpyrrolidone (PVP) in lead zirconate titanate (PZT) [31] and mullite [32] suspensions. Chen et al. [32] showed that critical cracking thicknesses were saturated above a certain concentration threshold of polyethylene oxide (PEO) in mullite dispersions with sol–gel reactions.

These descrepancies motivated the currrent investigation, wherein we demonstrate the multiple roles of polymeric additives in the cracking of drying colloidal suspensions. When polymer chains adsorb on particle surfaces, the polymers can act as a dispersant and stabilize the suspension through steric repulsive forces, thereby leading to homogenous close packing; thus, higher capillary stresses scaled on the surface tension divided by the radius of the free-surface curvature [33]. Nonadsorbing polymer chains in bulk fluids can become entangled or even gel with the help of a cross-linker [34], both of which can increase elastic stresses as polymer networks span across the films. However, the stress is reduced when polymers adsorb on air–liquid interfaces and act as surface-active agents to decrease the surface tension. Furthermore, polymeric additives can fill the interstitial spaces between neighboring particles and hinder the meniscus invasion above a critical concentration, leading to show a different stress development that is no longer driven by the capillarity.

Numerous studies have been reported on crack-morphology control via air blowing [35], electrostatic interactions among dispersing solids [36], the hydrophilic/hydrophobic surface patterning of the substrate [37-38], the addition of soft particles that deform to shrink pores between particles [39-41], constrained

geometry [42], and evaporation on elastomeric or liquid substrates on which the film shrinkage is no longer hampered by the adhesion on the substrate [28, 43]. However, it is not clearly evident how the adsorbing/nonadsorbing nature of polymeric additives on particle surfaces resist the crack propagation. Notwithstanding the facts that multicomponent suspensions are of broad relevance to colloidal science, the dominant physicochemical factors that determine the critical thickness in the presence of polymeric additives still remain unestablished.

Herein, we show evidence that the critical cracking thickness of an as-dried suspension increases in a non-linear, stepwise manner by increasing the adsorption amounts of polymeric additives on nanoparticle surfaces. The scaled critical thickness profile showed a single master curve trend with different particle diameters. We discuss the physical mechanism by combining the measured polymer adsorption amounts on particle surfaces, transitions in polymer chain conformations, and time-resolved drying stresses.

Experimental

Titanium dioxide (TiO_2) particles with the number-averaged diameter of 90 nm (F-1, Showa Denko) and 150 nm (F-10, Showa Denko) were dispersed in distilled water without the aid of surfactants. We used the scanning electron microscopy (JCM-7000 NeoScope, JEOL) to measure the particle size at a magnification of 70,000-100,000X and a voltage of 15 kV for secondary electron detector. The dry particles were mounted on a specimen stub using an electrically conductive double-sided adhesive tape and observed in high vacuum. The number-based particle size distribution was monomodal with standard deviations of 12 nm for

F-1 and 13 nm for F-10 particles, respectively. The polydispersities defined as the ratio of the volume-averaged to number-averaged particle diameter were 1.05 and 1.02 for the F-1 and F-10 particles. The specific surface areas of the particles were 19 and 11.5 m^2/g for the F-1 and F-10 particles, respectively. The zeta potential of the particle in the polymer-free suspension was measured using the zeta potential analyzer (ELSZ-2000, Otsuka Electronics Co. Ltd.) and found to be +2.2 mV. We used three different water-soluble polymeric additives: 98.0–99.0 mol% hydrolyzed poly(vinyl alcohol) (PVA-1, Kurary Co.) with a degree of polymerization of n = 1,700; 96.0 mol% hydrolyzed PVA-2 (Wako) with n = 500; and polyethylene glycol (PEG, Honeywell Fluka) with an average molecular weight of M_n = 20,000, as received. The PVA powders were dissolved in distilled water and stirred at temperatures above 333 K to obtain a homogenous polymer solution. Subsequently, the TiO_2 suspension was slowly added to the PVA solution, and stirred for 10 min using a supersonic homogenizer (Sonicstar85, Violamo, 21 ± 1kH). All the polymer–particle suspensions were continuously stirred for 20 h before use in the drying experiment. The initial particle volume fraction (ϕ) was fixed at 4.2 or 8.1 vol %, whereas the binder-to-particle mass ratio ranged between 0–0.092, corresponding to polymer mass fractions lower than 1.4 wt% at ϕ = 4.2 vol%.

The prepared suspension was cast onto a glass Petri dish with a diameter of 10 cm. The dish was inclined at 0.5–1° in the horizontal direction and mounted on a conductive heater (MP-3000HP, Kitazato) to maintain a bottom temperature of 333 K. The liquid sample with a wet-thickness gradient was dried in an air-shielded chamber at 30–50%RH. As drying occurred, an opaque region appeared in the thinner region and expanded toward the thicker region, thus leaving isolated

or interconnected cracks in certain areas with thicknesses above a critical value. We scanned the dried film surface via optical microscopy (VH-5900, Keyence Co. Ltd.) to determine the positions where the propagation length of visible cracks became shorter than 30 μm. The local dry thicknesses at the five pre-determined different positions were measured using a confocal laser displacement meter (LT8110, Keyence Co. Ltd.) and averaged to obtain the critical cracking thickness with an uncertainty of 2 μm.

To measure the adsorption isotherm of the polymeric additive on the particle surface, the suspension in a 2 mL tube was set up on a tabletop high-speed micro-centrifuge (CT15RE, Hitachi) and centrifuged at 1500 rpm (21,500 g) at 25 °C where g represents the gravitational acceleration. The supernatant with a controlled volume was extracted and dried to determine the residual polymer mass (m_p) with an accuracy of ± 0.01 mg. Assuming that the polymer concentration of the supernatant was equal to that of the polymer solution that filled the interstitial spaces between the particles in the sediment, the mass balance before and after the centrifugation enabled us to determine the amounts of adsorbed polymers on the particle surface. The adsorption amount measurements were repeated several times for suspensions with the same composition to ensure the accuracy of the measurements. The measured adsorption amount (Γ) in the unit of mg-PVA/m^2-TiO_2 complied with the power-law relation with respect to the polymer molecular weight (M) as $\Gamma \propto M^{\alpha}$. The adsorption amount is proportional to the molecular weight as $\alpha = 1$ when a polymer *brush* adsorbs on a particle surface at one end of the segment and stretches perpendicular to the surface. In the alternative case of a planar chain conformation along the particle surface, the number of adsorption sites occupied by the chains is independent of the polymer molecular weight once

the polymer adsorption amounts become identical; hence we obtain $\alpha = 0$. The polymer chain exhibits a loop–train conformation in the intermediate case of $0 < \alpha < 1$, where the *loop* denotes the stretch of segments where both ends are on the solid surface and the *train* denotes the sequences in contact with the surface [44].

To examine the drying-induced stress development, we used the in situ cantilever-beam deflection technique [45-46, and references therein]. The suspension was blade-coated onto a 0.5 mm thick glass cantilever (20 cm × 4 cm) with a Young's modulus and Poisson's ratio of E = 71.6 GPa and ν = 0.23, respectively. The initial wet thickness (c) was varied between 110 and 157 μm, and the particle volume fraction was fixed at ϕ = 8.1 vol%. The suspension was spread onto the cantilever surface with the coating area of 12 cm × 4 cm. The one end of the cantilever was clamped into the sample holder. The time variations in the end deflection of the cantilever were measured at 25 °C using a confocal laser displacement meter (LT8110, Keyence) at a sampling rate of 1 Hz. The laser focus was located at a pre-determined position on the uncoated substrate surface. A reflection of the laser light from the air-glass interface at the bottom surface of the glass substrate sometimes hampered the deflection measurement. To ensure the measurement accuracy, we selectively monitored the reflected light from the top surface using the confocal optical system. The stress was determined from the measured deflection using the Corcoran's equation [47] by assuming that: (i) the deflection was sufficiently small such that the coating surface profile was approximated by an arc and (ii) the modulus of the suspension was much smaller than that of the substrate:

$$\sigma = \frac{Et^3}{3cL^2(t+c)(1-\nu)}d. \quad (2)$$

where t and L denote the thickness and the length of the coated substrate, respectively. The coating bends as the stress develops, and the beam deflection relative to the initial position, d, varies in proportion to the stress (σ). It is worth noting that in-plane stress variations develop when drying first occurs at the edges of the substrate and then propagates inward from the edge. The deflection technique used in this work can measure only an average stress. Representative stress development curves are reported though several runs were conducted at each drying condition.

Results and Discussions

Figures 1a and 1b show the optical microscopy images of the typical examples of the dried film surface at different thicknesses. The suspension contained 90-nm-diameter TiO_2 particles and PVA with a degree of polymerization of n = 1700. The initial polymer mass fraction and the particle volume fraction were 0.12 wt%, and 4.2 vol%, respectively. Visible cracks are indicated by the arrows in the figures. Hair cracks propagated and intersected the neighboring cracks in the 30 μm thick films (Fig. 1a), whereas the cracks were shortened and isolated at a lower thickness near the critical cracking thickness of h_{CCT} = 19.2 μm (Fig. 1b). The cracks became shorter and eventually became invisible as the thickness decreased below the critical cracking thickness. Our supplemental measurements on a horizontal substrate showed the same critical cracking thickness as that on the inclined substrate.

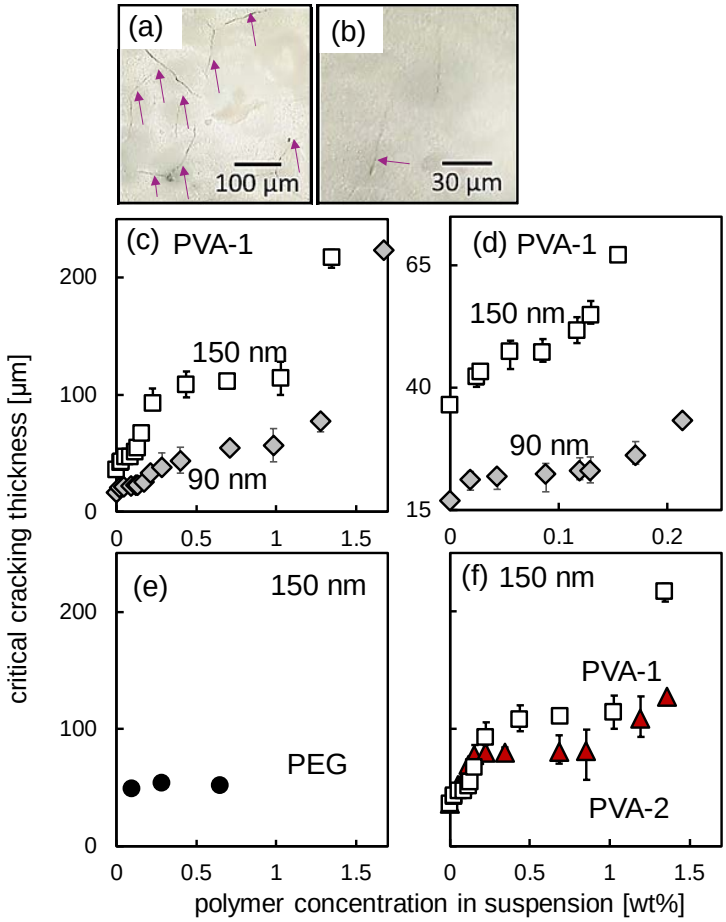

Fig.1 Optical microscopy images of the dried film surface at different thicknesses of (a) 30 μm and (b) 19.2 μm. The suspension contained TiO_2 particles with diameters of 90 nm and poly(vinyl alcohol)(PVA) with the degree of polymerization of n = 1,700. and it was dried at 60 ºC on the inclined substrate. Critical cracking thickness of (c) PVA-1 suspensions for two particle diameters, (e) poly(ethyleneglycol) suspensions, and (f) PVA-2 suspensions with lower molecular weight. (d) Magnified image of Fig. 1c to emphasize the presence of the first plateau of the critical thickness at low polymer concentrations.

We systematically examined how the critical cracking thickness varied with the particle diameter, initial polymer concentrations, polymer species, and the

molecular weight of the polymer. Figures 1c and 1d illustrate the measured critical thicknesses of PVA-1 suspensions for two different particle diameters. An increase in the initial polymer concentration resulted in a stepwise increase in the critical cracking thickness as follows: the critical thickness first increased, reached the first and the second plateaus, and then diverged to infinity above a critical polymer concentration. Fig. 1d shows the magnified image of Fig. 1c to emphasize the existence of the first plateau of the critical thickness at low polymer concentrations. To the best of our knowledge, such a nonlinear but monotonic increase in the critical cracking thickness has not been reported previously. The results also revealed that the critical cracking thickness for the suspension of larger particles (open symbol) was higher than that for smaller particles (closed symbol). This is qualitatively consistent with the theoretical prediction [27] for the critical thickness of polymer-free suspensions, i.e., $h_{CCT} \propto D_p^{3/2}$, where D_p denotes the particle diameter. Nonetheless, the critical thickness of the PEG suspension was rather independent of the polymer concentration and much lower than that of the PVA-1 suspensions, even at the same particle diameter (Fig. 1e). A comparison between the PVA-1 and PVA-2 suspensions revealed that the critical cracking thicknesses converged into a single band at low polymer concentrations; the PVA-1 suspension exhibited a larger critical cracking thickness value compared to that of the PVA-2 suspension at high concentrations, indicating that longer polymer chains can suppress cracking into thicker films (Fig. 1f).

To understand the composition-dependent variations in the critical cracking thickness, we compared the adsorption isotherms of PVA-1, PVA-2, and PEG on the TiO_2 particle surface at 25 °C. The mass fraction and diameter of the particles were fixed at 15 wt% and 150 nm, respectively. Fig. 2a shows the adsorption

amounts of the polymer plotted against the mass of the polymer per unit surface area of the particles. The solid line represents the adsorption amounts when the total amount of the polymeric additive (C_{total}) agrees with the adsorption amounts (Γ) onto the particle surface, i.e., the amounts of nonadsorbing polymers are negligible small in the suspension.

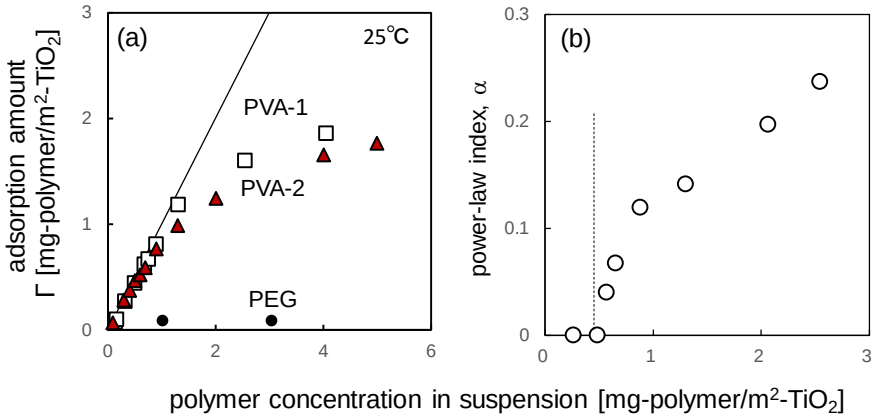

Fig. 2 (a) Adsorption isotherms of PVA-1, PVA-2, and PEG suspensions at 25 °C. The particle diameter and mass fraction were 150 nm and 15wt%, respectively. The adsorption amounts (Γ) monotonically increase with the concentrations of PVA-1 and PVA-2, whereas they retain a constant value in PEG suspension. (b) Power-law index for the relationship between the adsorption amounts and the polymer molecular weight (M) as $\Gamma \propto M^{\alpha}$. The index was approximately zero at concentrations below the critical polymer concentration of 0.4 mg-PVA/m^2-TiO_2, whereas it increased to show positive, non-zero values at higher concentrations.

The measured adsorption amounts of PVA-1 linearly increased with the polymer concentration and complied with a simple relationship, i.e., Γ/C_{total} ~1, at low concentrations below the critical concentration of 0.4 mg-PVA/m^2-TiO_2. The adsorption amounts of PVA-1 tended to saturate at higher concentrations, showing a Langmuir-type adsorption isotherm. In the case of PVA-2 with a lower molecular weight, the adsorption amounts exhibited the same linear relationship below the critical concentration but exhibited lower values compared to those of PVA-1 at higher concentrations. To address the molecular-weight dependence, we fitted the data with a power-law, $\Gamma \propto M^{\alpha}$, and determined the index (α) where M denotes the polymer molecular weight. The index was approximately zero at low concentrations, whereas it showed positive values of less than unity above a certain threshold corresponding to the critical adsorption amount of Γ_c = 0.4 mg-PVA/m^2-TiO_2 (Fig. 2b). This shift from zero to a non-zero index indicates a transition from the planar to loop–train-like configurations of PVA molecules on the particle surface. When the polymer chains adsorb along the surface at low concentrations, the adsorption amount becomes independent of the polymer molecular weight, i.e., $\alpha = 0$, although there have been many debates on whether all polymer segments extend along a solid surface [48]. The non-zero index at higher concentrations indicates an intermediate state of polymer chains between two extremes of planar ($\alpha = 0$) and brush ($\alpha = 1$) conformations on the particle surface.

However, the PEG adsorption amounts were much lower than those of PVA, indicating a near-constant value regardless of the polymer concentrations. As mentioned above, the addition of PEG had little influence on the critical cracking thickness (Fig. 1e). These results imply that polymer adsorption onto particle

surfaces plays a role in delaying crack nucleation to thicker particulate films. This result was qualitatively consistent with that reported by Kumano et al. [12], who demonstrated that crack behavior was controlled by ionomer adsorption in Pt/carbon catalyst inks.

To clarify the effects of polymer adsorption on cracking, we replotted the critical cracking thickness against the polymer adsorption amounts in suspensions. A typical example of the h_{CCT}–Γ curve for the PVA-1 suspension containing 150 nm diameter particles is shown in Fig. 3. The critical cracking thickness increased, reached the first plateau, and then increased again with the adsorption amounts of the polymer. The onset of the second increase in the critical cracking thickness emerged above the critical amount of Γ_c = 0.4 mg-PVA/m^2-TiO_2, which agreed well with that at the transition from the planar-like (Regime I) to loop–train (Regime II) conformations of the adsorbing polymer chain (Fig. 2b), thereby suggesting adsorption-mediated variations in the critical cracking thickness.

As mentioned previously, the development of tensile stress is the origin of crack propagation. To understand how the polymeric additive influences stress evolutions below or above the critical adsorption amount, we conducted time-resolved stress measurements of the drying suspension using the cantilever-beam deflection method. Typical examples of stress evolutions are shown in Fig. 4 for suspensions with the initial thicknesses of c = 139±1 μm. The initial thickness was chosen to be below the critical cracking thickness because a crack propagation sometimes inhibits the reproducibility of the measurements.

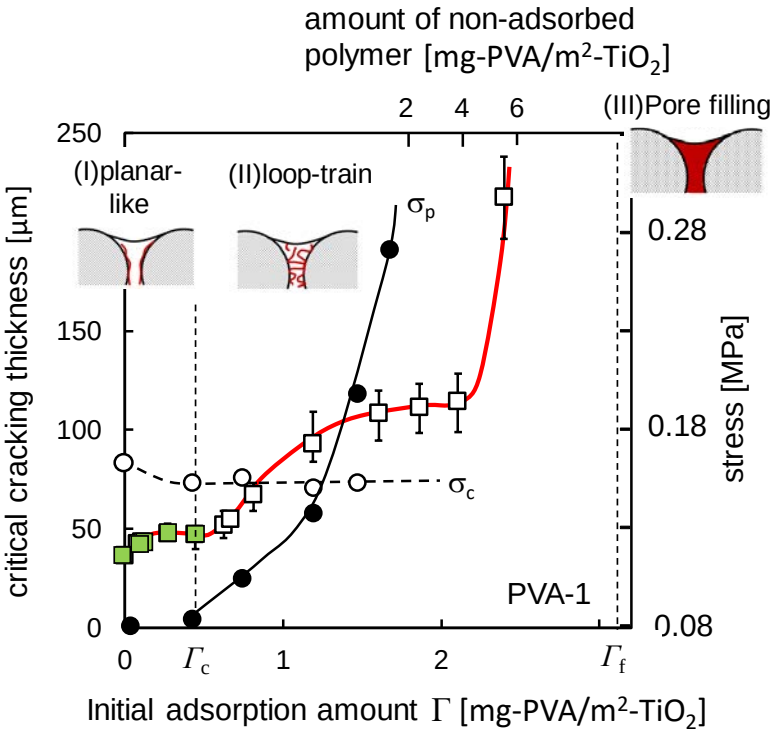

Fig. 3 Variations in the critical cracking thickness and the stress with different PVA adsorption amounts on the TiO_2 particle surface. The suspension contained 15wt% TiO_2 particles with a diameter of 150 nm and PVA with a degree of polymerization of n = 1,700, and it was dried at 60 ºC. The closed and open rectangle symbols represent the critical thicknesses in concentration ranges where the adsorbing polymers exhibit planar-like and loop–train configurations, respectively. The critical thickness of the polymer-free suspension was 35.4 μm.

In suspensions with concentrations below the critical polymer concentration, the built-up stress reached a maximum at a certain drying time (t^*), and then relaxed, leaving a finite residual stress after drying was completed. We attributed the peak stress to the capillary pressures generated when the menisci invaded the packing layer of the particles [1]. To compare the stress evolutions at different compositions, the drying time (t) was considered to be dimensionless with respect to the time at the stress peak as t/t^*. As we increased the initial concentration of

the polymeric additives, the first increase in stress was followed by the evolution of the second stress in the latter drying stages, thereby showing a good qualitative agreement with previous stress measurements [49-50]. The magnitude of the stress level at the second peak increased with increasing the polymer concentration, leaving residual stresses that are much higher than those in the polymer-free suspensions.

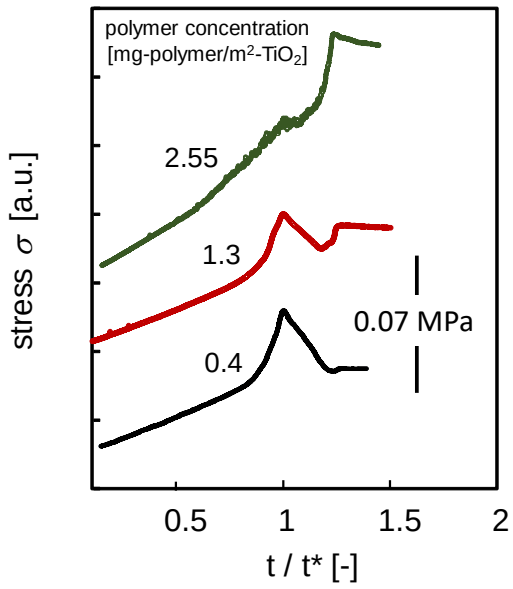

Fig. 4 Time evolutions in the cantilever deflection of suspensions with different polymer concentrations. The polymer-free suspension exhibits a single stress peak, whereas the secondary stress peak increases with polymer concentrations. The initial suspension thickness was 139±1.3 μm, which was chosen to be below the critical cracking thickness at any polymer concentrations.

To examine the physical interplay between the stress and crack evolutions, we focused on two characteristic stresses: the capillary stress at the first peak (σ_c) and the residual polymer stress after drying was completed (σ_p), which are depicted as open and closed circles in Figure 3, respectively. The results revealed three distinct stress regimes. At low polymer contents below Γ_c (Regime I), the maximum stress slightly decreased with increase in the polymer adsorption amount and retained an approximately constant value of $\sigma_c \sim 0.17$ MPa. This stress agreed with the capillary stress estimated using the Laplace equation, $\gamma/r \sim 0.2$ MPa, by substituting the surface tension, $\gamma = 60$ mN/m, and the radius of meniscus curvature, $r \sim 300$ nm. The polymer stress was negligibly small compared to the capillary stress at $\Gamma < \Gamma_c$, which was consistent with the fact that nonadsorbing polymers barely exist in the bulk fluid (Fig. 2a).

With increasing polymer adsorption amounts above Γ_c, the capillary stress retained a constant value, whereas the polymer stress increased and eventually overcame the capillary stress, indicating a stress cross-over at $\Gamma \sim 1.2$ mg-PVA/m^2-TiO_2 (Regime II). The constant capillary stress indicates no significant change in the particle packing structures, despite the common observation that adsorbing polymers induce steric repulsive forces between neighboring particles to alter the final packing of particles [33]. The residual polymer stress significantly increased as we further increased the adsorption amounts above the cross-over point.

The increase in the polymer stress in Regime II can be understood by considering the entanglement of nonadsorbing polymer chains at high concentrations. The entangled chains create polymer networks, which span the

film and deform as the film shrinks, thereby inducing the stress evolution, particularly in the late drying stages (see Fig. 4). To check whether the polymer chains in the as-coated suspensions were entangled, we determined the entanglement concentration (c_e) of PVA-1 from the relation $\eta \sim c^n$, where c and η represent the polymer concentration and the viscosity of particle-free solution, respectively [51]. The slopes of the log η–log c plots changed at the critical concentration of c_e = 3 wt%, which was higher than the initial concentrations of non-adsorbed polymers. These findings implied that a transition from a semi-dilute unentangled to entangled states emerged via drying-induced compositional changes rather than an increase in initial polymer concentrations.

The entanglement of nonadsorbing polymer chains not only led to a higher elastic stress but also assisted in toughening the coating against the stress. When polymer chains interact with those on particle surfaces, the adsorbing/nonadsorbing chains would bridge the neighboring particles to increase the mechanical strength of the coating. The toughened coating involves a higher critical stress of cracking, and thus, it becomes robust against the drying-induced deformations. This was consistent with the fact that the critical cracking thickness increased with the polymer concentration in Regime II. The critical thickness was eventually saturated to show the secondary plateau at $\Gamma^* \sim 2$ mg-PVA/m^2-TiO$_2$, implying that the adsorption-mediated toughening balanced the stress buildup.

The critical cracking thickness significantly increased above the critical amount (Γ^*) and finally diverged, indicating the formation of crack-free films at high polymer contents (Regime III in Fig. 3). The divergence in the critical cracking thickness can be attributed to the structural transition from a porous particulate film into a composite, where particles are embedded in the polymer matrix. To

verify this, we estimated the critical polymer/particle volume ratio (r), above which polymers can fill the complete interstitial spaces between the particles. Assuming that the particle volume fraction, ϕ = 0.64, in the random-closed packing limit, we obtained r = 0.56, which corresponded to the polymer adsorption amount of Γ_f = 3.1 mg-PVA/m^2-TiO_2. This critical amount (Γ_f) was marginally higher than, but in the same order as, the critical adsorption amount by which the critical cracking thickness diverged, thereby implying that the filling of the interparticle spaces by the polymeric additives hindered the meniscus invasion and delayed cracking into much thicker films.

It is imperative to obtain h_{CCT}–Γ master curves to design drying processes by which crack-free particulate coatings can be fabricated. A previous theory [27] for polymer-free suspensions has reported that the critical thickness complies with $h_{CCT} \propto (GD_p^3/\gamma)^{1/2}$, where D_p denotes the particle diameter, G is the shear modulus of the particle, and γ is the liquid–air surface tension. Herein, we adopt this scaling to the suspensions containing polymeric additives, as shown in Fig. 5. The polymer adsorption amounts were made dimensionless using the critical value Γ_f, above which all particles were embedded in the polymer matrix. The scaled critical thickness $h_{CCT}/(GD_p^3/\gamma)^{1/2}$ converges into a single band at different particle diameters and polymer concentrations, indicating that this master curve facilitates the prediction of the critical cracking thickness once the adsorption isotherm of a given suspension of interest is obtained.

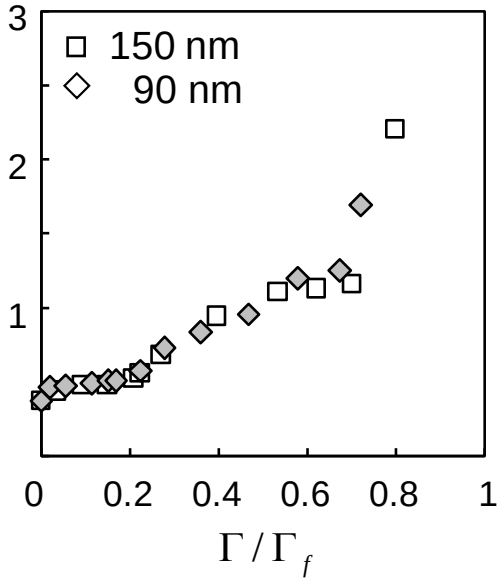

Fig. 5 Master curve of the critical cracking thickness (h_{CCT}) of PVA-1 suspensions plotted against normalized polymer adsorption amounts on the particle surfaces. The initial particle mass fraction was 15 wt% (particle volume fraction of ϕ = 4.2 %). The critical thickness scaled by $(GD_p^3/\gamma)^{1/2}$ converged into a single non-linear curve at different particle diameters (D_p) and polymer contents. We assumed a constant modulus and surface tension as $G/\gamma = 2.9\times10^{12}$ m^{-1}.

It is not clearly evident how the $h_{CCT}-\Gamma$ curve depends on the molecular structures, adsorption kinetics on particle surfaces, and the elastic nature of polymeric additives. Recently, Koga and Inasawa [52] demonstrated that partially saponified PVA suppressed cracking at lower polymer concentrations compared to fully saponified PVA, suggesting that functional groups alter the critical conditions of cracking. Their results are qualitatively consistent with the adsorption-mediated cracking presented in this study because the partially saponified PVA contained less hydroxyl (-OH) groups and was readily adsorbed on the surface of silica particles [33, 52]. However, thus far, no theoretical

framework has been developed to predict the critical cracking thicknesses for polymers with different functional groups. Further studies are needed to explore the microscopic mechanism to explain how the transition in polymer chain conformations on particle surfaces changes the packing of particles and the interactions between the adsorbing and nonadsorbing polymer chains, both of which can affect the stress evolutions and, consequently, the critical cracking thickness. Nevertheless, this study provides a practical basis toward attaining a fundamental understanding of how the adsorbing/nonadsorbing nature of polymeric additives play the multiple roles in suppressing crack propagation in drying colloidal suspensions.

Conclusions

We showed experimental evidence that the critical cracking thickness (h_{CCT}) of as-dried nanoparticle suspensions increased in a stepwise manner with increasing concentrations of polymeric additives. This nonlinearity in the critical cracking thickness was attributed to the multiple roles played by the additives including (i) the onset of polymer adsorption on the nanoparticle surface, (ii) transition from planar to the loop–train in conformations of polymer chains on particles, (iii) the chain entanglements of nonadsorbing polymers in bulk fluids, and (iv) the filling of pores between neighboring particles, depending on the particle diameters (D_p), polymer molecular weights, and initial polymer concentrations in suspensions. The same scaling used in additive-free suspensions, i.e., $h_{CCT} \propto D_p^{3/2}$, was found to be applicable in PVA–TiO_2 aqueous suspensions despite the different physical origins of delayed cracking into thicker films.

Acknowledgment

The author wishes to thank Takuya Tahara and Shuhei Kubo for their technical assistance with the experiments. The author acknowledges the financial support of the Japan Society for the Promotion of Science (JSPS) KAKENHI (20H02507) Grant-in-Aid for Scientific Research B.

References

1. Chiu RC, Cima MJ. Drying of Granular Ceramic Films; II, Drying stress and saturation uniformity, Journal of American Ceramic Society, 1993; 76: 2769-2777.
2. Giorgiutti-Dauphin´e F, Pauchard L. Elapsed time for crack formation during drying, The European Physical Journal E, 2014; 37:39. DOI: 10.1140/epje/i2014-14039-8. Epub 2014 May 26. PMID: 24853634.
3. Jing G, Ma J. Formation of circular crack pattern in deposition self-assembled by drying nanoparticle suspension, Journal of Physical Chemistry B, 2012; 116:6225-6231.
4. Yang B, Sharp JS, Smith MI. The interplay of crack hopping, delamination and interface failure in drying nanoparticle films, Scientific Reports, 2016; 6:32296.
5. Yamamura M, Ono H, Uchinomiya T, Mawatari Y, Kage H. Multiple crack nucleation in drying nanoparticle-polymer coatings, Colloids and Surfaces A: Physicochemical and Engineering Aspects, 2009;342: 65-69.

6. Allain C, Limat L. Regular patterns of cracks formed by directional drying of a colloidal suspension, Physical Review Letters, 1995;74: 2981-2984.
7. Chen K, Taflove A, Kim YL, Backman V. Self-assembled patterns of nanospheres with symmetries from submicrons to centimeters, Applied Physics Letters, 2005;86: 033101-1-033101-3.
8. Dufresne ER, Corwin EL, Greeblatt NA, Ashmore J, Wang DY, Dinsmore AD, Cheng JX, Xie XS, Hutchinson JW, Weitz DA. Flow and fracture in drying nanoparticle suspensions, Physical Review Letters, 2003;91: 224501-1-224501-4.
9. Inasawa S, Oshimia Y, Kamiya H. Formation kinetics of particulate films in directional drying of a colloidal suspension, Soft Matter, 2016;12: 6851-6857.
10. Weldon AL, Joshi K, Routh AF, Gilchrist JF. Uniformly spaced nanoscale cracks in nanoparticle films deposited by convective assembly, Journal of Colloid and Interface Science, 2017; 487: 80-87.
11. Ahn CY, Jang S, Cho YH, Choi J, Kim S, Kim SM, Sung YE. Choi M. Guided cracking of electrodes by stretching prism-patterned membrane electrode assemblies for high-performance fuel cells, Scientific Reports, 2018;8:1257 DOI:10.1038/s41598-018-19861-6.
12. Kumano N, Kudo K, Suda A, Akimoto Y, Ishii M, Nakamura H. Controlling cracking formation in fuel cell catalyst layers, Journal of Power Sources, 2019; 419: 219-228.
13. Ahn K, Kim D, Kim O, Nam J. Analysis of transparent conductive silver nanowire films from dip coating flow, Journal of Coatings Technology and Research, 2015; 12: 855-862.

14. Lewis JA, Blackman KA, Ogden AL, Payne JA, Francis LF. Rheological property and stress development during drying of tape-cast ceramic layers, Journal of American Ceramic Society, 1996; 79: 3225-3234.
15. Kiennemann J, Chartier T, Pagnoux C, Baumard JF, Huger M, Lamerant JM, Drying mechanisms and stress development in aqueous alumina tape casting, Journal of European Ceramic Society, 2005; 25: 1551-1564.
16. Tirumkudulu MS, Russel WB. Cracking in drying latex films, Langmuir, 2005;21: 4938-4948.
17. Lan W, Xiao P, Drying stress of yttria-stabilized-zirconia slurry on a metal substrate, Journal of the European Ceramic Society, 2007; 27: 3117-3125.
18. Lim S, Kim S, Ahn KH, Lee SJ. Stress development of Li-ion battery anode slurries during the drying process, Industrial & Engineering Chemistry Research, 2015; 54: 6146-6155.
19. Wu Y, Francis LF, Effect of particle size distribution on stress development and microstructure of particulate coatings, Journal of Coatings Technology and Research, 2017; 14: 455-465.
20. Sengupta R, Tirumkudulu MS. Dynamics of cracking in drying colloidal sheets, Soft Matter, 2016; 12: 3149-3155.
21. Xu Y, German GK, Mertz AF, Dufresne ER. Imaging stress and strain in the fracture of drying colloidal films, Soft Matter, 2013; 9: 3735-3740.
22. Tirumkudulu MS, Russel WB. Role of capillary stresses in film formation, Langmuir, 2004; 20: 2947-2961.
23. Lee WP, Routh AF. Why do drying films crack, Langmuir 2004; 20: 9885-9888.

24. Routh AF, Russel WB. A process model for latex film formation: limiting regimes for individual driving forces, Langmuir, 1999; 15: 7762-7773.
25. Chekchaki M, Lazarus V, Mechanical stresses induced by evaporation in consolidated colloidal suspensions of hard particles. Poroelasticity theory versus experiments, Transport in Porous Media, 2013; 100:143-157.
26. Griffith AA. The phenomena of rupture and flow in solids, Philosophical Transactions of the Royal Society London A, 1921; 221: 163-198.
27. Singh KB, Tirumkudulu M. Cracking in drying colloidal films, Physical Review Letters, 2007; 93: 218302.
28. Chiu RC, Garino TJ, Cima MJ. Drying of granular ceramic films; I, effect of processing variables on cracking behavior, Journal of American Ceramic Society, 1993;76: 2257-2264.
29. Qiao J, Adams J, Johannsmann D. Addition of halloysite nanotubes prevents cracking in drying latex films, Langmuir, 2012;28: 8674-8680.
30. Schneider M, Maurath J, Fischer SB, Weis M, Willenbacher N, Koos E. Suppressing crack formation in particulate systems by utilizing capillary forces, ACS Applied Materials & Interfaces, 2017;9: 11095–11105.
31. Kozuka H, Takenaka S. Single-step deposition of gel-derived lead zirconate titanate films: critical thickness and gel film to ceramic film conversion, Journal of the American Ceramic Society, 2002; 85: 2696-2702.
32. Chen Z, Burtovyy R, Kornev K, Luzinov I, Xu D, Peng F. The effect of polymer additives on the critical thicknesses of mullite thin films obtained from the monophasic sol-gel precursors, Journal of Sol-Gel Science and Technology, 2016; 80:285-296.

33. Kim, S., Sung J.H., Chun, S., Ahn, K.H., Lee, S.J., Adsorption-stress relationship in drying of silica/PVA suspensions, Journal of Colloid and Interface Science, 2011; 261: 497-502.
34. Carreras, E.S., Chabert, F., Dunstan, D.E., Franks, G.V., Avoiding "mud" cracks during drying of thin films from aqueous colloidal suspensions, Journal of Colloid and Interface Science, 2007; 313: 160-168
35. Yamamura M. Ono H., Uchinomiya, T., Mawatari Y., Kage H., Suppressed cracking in drying nanoparticle-polymer coatings at high Peclet numbers, Journal of Chemical Engineering of Japan, 2010; 43: 209-213.
36. Mailer AG, Clegg PS, Cracking in films of titanium dioxide nanoparticles with varying interaction strength, Journal of Colloid and Interface Science, 2014; 417: 317-324.
37. Sun W, Jia F, Sun Z, Zhang J, Li Y, Zhang X, Yang B. Manipulation of cracks in three-dimensional colloidal crystal films via recognition of surface energy patterns: an approach to regulating crack patterns and shaping microcrystals, Langmuir, 2011; 27: 8018-8026.
38. Shorlin, KA, de Bruyn JR, Graham M, Morris SW. Development and geometry of isotropic and directional shrinkage-crack patterns, Physical Review E, 2000; 60: 6950-6957.
39. Roberts CC, Francis LF. Drying and cracking of soft latex coatings, Journal of Coatings Technology and Research, 2013; 10: 441-451.
40. Jin Q, Tan P, Schofield AB, Xu L. Eliminating cracking during drying, The European Physical Journal E, 2013; 36:28 DOI: 10.1140/epje/i2013-13028-9.

41. van der Kooij HM, de Kool M, van der Gucht J, Sprakel J. Coalescence, cracking, and crack healing in drying dispersion droplets, Langmuir, 2015; 31: 4419-4428.
42. Han W, Li B, Lin Z. Drying-mediated assembly of colloidal nanoparticles into large-scale microchannels, ACS Nano, 2013; 7: 6079-6085.
43. Smith MI, Sharp JS. Effects of substrate constraint on crack pattern formation in thin films of colloidal polystyrene particles, Langmuir, 2011; 27: 8009-8017.
44. Scheutjens JMH, Fleer GJ. Statistical theory of the adsorption of interacting chain molecules.1. Partition function, segment density distribution, and adsorption isotherms, The Journal of Physical Chemistry, 1979; 83: 1619-1635.
45. Francis LF, McCormick AV, Vaessen DM, Payne JA. Development and Measurement of Stress in Polymer Coatings, Journal of Materials Science, 2002; 37:4717-4731.
46. Price KK, Wu Y, McCormick AV, Francis L. Stress development in hard particle coatings in the absence of lateral dying, Journal of American Ceramic Society, 2015; 98: 2214-2222.
47. Corcoran EM, Determining stresses in organic coatings using plate beam deflection, Journal of Paint Technology, 1969; 41: 635-640.
48. Kawaguchi M, Hayakawa K, Takahashi A. Adsorption of polystyrene onto a metal surface in good solvent conditions, Macromolecules, 1983; 16: 631-635.
49. Petersen C, Heldmann C, Johannsmann D, Internal Stresses during Film Formation of Polymer Latices, Langmuir, 1999; 15: 7745-7751.

50. Wedin P, Lewis JA, Bergstrom L. Soluble organic additive effects on stress development during drying of calcium carbonate suspensions, Journal of Colloid and Interface Science, 2005; 290: 134-144.
51. Colby RH, Fetters LJ, Funk WG, Graessley WW. Effects of concentration and thermodynamics interaction on the viscoelastic properties of polymer solutions. Macromolecules, 24; 1991: 3873-3882.
52. Koga S, Inasawa S, Packing structures and formation of cracks in particulate films obtained by drying colloid-polymer suspensions, Colloids and Surfaces A, 2019; 563: 95-101.

List of Figures

loop–train configurations, respectively. The critical thickness of the polymer-free suspension was 35.4 μm.

Fig. 4 Time evolutions in the cantilever deflection of suspensions with different polymer concentrations. The polymer-free suspension exhibits a single stress peak, whereas the secondary stress peak increases with polymer concentrations. The initial suspension thickness was 139 ± 1.3 μm, which was chosen to be below the critical cracking thickness at any polymer concentrations.

Fig. 5 Master curve of the critical cracking thickness (h_{CCT}) of PVA-1 suspensions plotted against normalized polymer adsorption amounts on the particle surfaces. The initial particle mass fraction was 15 wt% (particle volume fraction of ϕ = 4.2 %). The critical thickness scaled by $(GD_p^3/\gamma)^{1/2}$ converged into a single non-linear curve at different particle diameters (D_p) and polymer contents. We assumed a constant modulus and surface tension as $G/\gamma = 2.9 \times 10^{12}$ m^{-1}.